iScience

CellPress
OPEN ACCESS

Article

The temporal pattern of synaptic activation determines the longevity of structural plasticity at dendritic spines

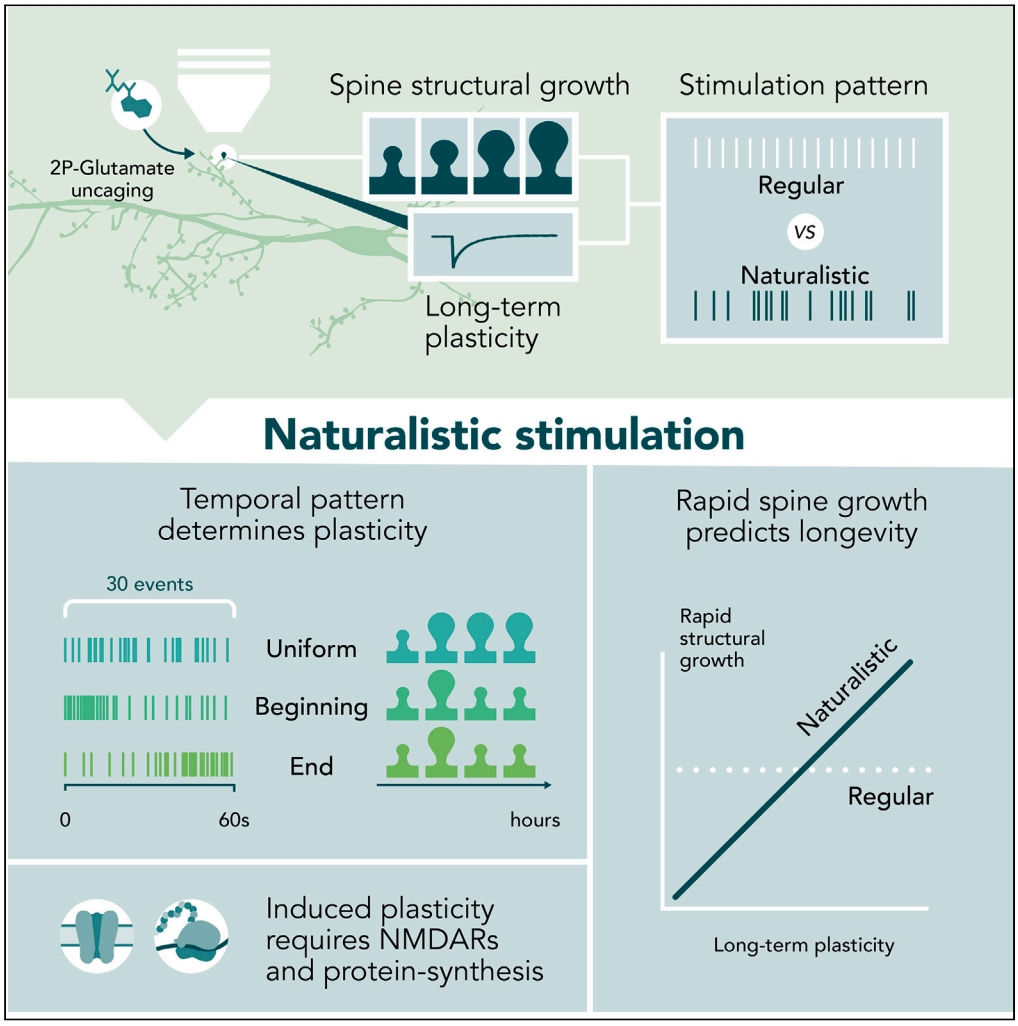

Ali Özgür Argunsah, Inbal Israely

argunsah@hifo.uzh.ch (A.Ö.A.)
inbal@uw.edu (I.I.)

Highlights

The pattern of the naturalistic stimulation determines the longevity of plasticity

Plasticity induced by naturalistic patterns requires NMDARs and protein synthesis

Spine growth during naturalistic stimulation predicts the longevity of the plasticity

Argunsah & Israely, iScience 26, 106835
June 16, 2023
https://doi.org/10.1016/j.isci.2023.106835

iScience

CellPress
OPEN ACCESS

Article

The temporal pattern of synaptic activation determines the longevity of structural plasticity at dendritic spines

Ali Özgür Argunsah[1,2,3,*] and Inbal Israely[1,4,5,6,*]

SUMMARY

Learning is thought to involve physiological and structural changes at individual synapses. Synaptic plasticity has predominantly been studied using regular stimulation patterns, but neuronal activity in the brain normally follows a Poisson distribution. We used two-photon imaging and glutamate uncaging to investigate the structural plasticity of single dendritic spines using naturalistic activation patterns sampled from a Poisson distribution. We showed that naturalistic activation patterns elicit structural plasticity that is both NMDAR and protein synthesis-dependent. Furthermore, we uncovered that the longevity of structural plasticity is dependent on the temporal structure of the naturalistic pattern. Finally, we found that during the delivery of the naturalistic activity, spines underwent rapid structural growth that predicted the longevity of plasticity. This was not observed with regularly spaced activity. These data reveal that different temporal organizations of the same number of synaptic stimulations can produce rather distinct short and long-lasting structural plasticity.

INTRODUCTION

Information is believed to be encoded at the cellular level through activity-dependent alterations in synaptic weights, which are correlated with structural modifications of dendritic spines.[1,2] These are the major sites where excitatory synapses are located and their morphology is highly regulated by incoming activity.[3,4] Through two-photon imaging and glutamate uncaging, neuronal structure and function can be probed with high temporal and spatial resolution at single synapses, allowing for the identification of a linear relationship between the synaptic current and the volume of the spine on which it is measured.[5,6] Furthermore, the light-mediated release of regularly spaced pulses of glutamate induces both synaptic potentiation and long-lasting spine growth at single spines demonstrating that changes in spine size can be used as a proxy for functional plasticity.[1,7,8] Such structural plasticity can either be short- or long-lasting, depending on the availability of plasticity related proteins,[8] similar to the case during functional plasticity.[9–11]

Much of our understanding of synaptic plasticity rules has been achieved through the delivery of regularly spaced temporal patterns of activity, such as high- or low-frequency stimulation trains.[12–14] Activity in the brain is organized differently, and firing patterns are more accurately captured by Poisson-like distributions, in which spiking events occur independently over time with intervals spanning an exponential range.[15–18] Indeed, the response properties of single neurons and local circuits are fundamentally different for regularly spaced stimuli compared to naturalistic or noisy stimuli.[19–22] Yet it is unknown how patterns of endogenous activity relate to structural plasticity at single inputs.

Therefore, we aimed to determine the structural plasticity consequences of naturalistic based patterns of activity at single spines. We developed optical stimulation paradigms with Poisson timing structures to mimic the irregularity of endogenous activity in the hippocampus. We used two-photon glutamate uncaging and imaging to deliver these patterns to single dendritic spines in CA1 pyramidal neurons and tracked the resulting structural plasticity over different time scales. We found that the temporal pattern of activation determines the longevity of plasticity, indicating that single dendritic spines integrate transient information into either short or long-lasting structural plasticity in an activity-dependent manner. The critical variable which gave rise to this difference in plasticity was in the temporal distribution of the patterns: when stimuli were spread evenly across the epoch they induced more robust plasticity, whereas those with stimuli massed toward either the beginning or the end of the patterns were less efficient at inducing sustained structural plasticity. We also observed that across the population of potentiated spines, the

[1]Champalimaud Research, Champalimaud Centre for the Unknown, 1400-038 Lisbon, Portugal

[2]Laboratory of Neuronal Circuit Assembly, Brain Research Institute (HiFo), University of Zurich, Winterthurerstrasse 190, 8057 Zürich, Switzerland

[3]Neuroscience Center Zurich (ZNZ), Winterthurerstrasse 190, 8057 Zürich, Switzerland

[4]Department of Pathology and Cell Biology, Department of Neuroscience, in the Taub Institute for Research on Alzheimer's Disease and the Aging Brain, Columbia University Medical Center, Vagelos College of Physicians and Surgeons, Columbia University, New York, NY 10032, USA

[5]Present address: Department of Physiology and Biophysics, University of Washington School of Medicine, Seattle, WA 98195, USA

[6]Lead contact

*Correspondence: argunsah@hifo.uzh.ch (A.Ö.A.), inbal@uw.edu (I.I.)

https://doi.org/10.1016/j.isci.2023.106835

degree of structural growth during these stimulations varied and was highly predictive of the endurance of the structural plasticity that spines would express. Thus, we revealed that structural plasticity can occur extremely rapidly and that early changes during naturalistic activity are predictive of longevity. Finally, we determined that the induction of structural plasticity by these patterns requires activity through NMDA receptors, as well as new protein synthesis, confirming the involvement of known synaptic plasticity mechanisms for the expression of long-lasting structural modifications. Thus, we demonstrate for the first time that naturalistic based stimulation patterns can elicit plasticity at single inputs and that the robustness of the resulting plasticity is dependent on the temporal organization of activity.

RESULTS

The temporal structure of naturalistic stimulation patterns determines the longevity of plasticity

A widely used paradigm for the induction of long-term potentiation (LTP) at single spines involves light-mediated delivery of 30 pulses of glutamate[7,8,23–26] (4 ms-long pulse-width, at 0.5 Hz, lasting 60 s), which we will refer to as 30-Reg (Reg: Regularly spaced). We wanted to establish a naturalistic-based uncaging stimulation pattern that we could compare to the known structural and functional outcomes of the 30-Reg stimulation. We chose paradigms with timing structures that follow a Poisson distribution, as the irregularly structured nature of endogenous activity in the hippocampus is well modeled by this distribution.[27] It is also consistent with the range of firing schemes observed in behaving animals in CA3 pyramidal neuron populations, which provide input to CA1 dendrites.[17] We sampled multiple temporal patterns from a homogeneous Poisson process (HPP) with an expected number of events equal to 30, to approximate our standard paradigm ($\lambda = 30$, Figure 1A, see STAR Methods for details). Among this distribution, we selected only those patterns containing exactly 30 pulses, to match our established plasticity protocol, as well as to control that the same total amount of glutamate would be delivered over the stimulation window across paradigms. Owing to the probabilistic nature of the Poisson sampled patterns, only 740 patterns out of the 10,000 generated had exactly 30 pulses in 60s (Figure 1A inset). We sorted the patterns according to how events were distributed over three equal time bins: either a pattern contained a pseudo-uniform distribution (with 10 pulses in each 20s bin), or pulses were skewed toward occurring predominantly at the beginning or end of the stimulation period (during the first or last 20s bin). We refer to these patterns as naturalistic stimulation patterns (NSP), and we selected one representative from each group: NSP-Uniform (NSP-Uni), NSP-Beginning (NSP-Beg), and NSP-End, respectively (Figures 1B and S1). Thus, we had one homogeneously distributed Poisson pattern (NSP-Uni) and two non-homogeneously distributed Poisson patterns (NSP-Beg and NSP-End) that emerged from the same distribution, which we next used to evaluate structural plasticity at single spines. Before starting plasticity experiments, we considered the possibility that as some of the inter-pulse-intervals in the NSP trains were short (for example, 34 ms compared to 2000 ms in the 30-Reg pattern), the NSP protocols may effectively be delivering fewer stimuli and thus less glutamate signaling, compared to their more distributed counterparts. To test whether the non-regular paradigms produce responses to each of the 30 pulses, we conducted a set of experiments in which whole-cell patch-clamp recordings were carried out during the NSP stimulations. For a given pattern, we validated that each uncaging pulse produced a corresponding uncaging-mediated excitatory postsynaptic current (uEPSC) that could be detected at the soma of the neuron as a discrete event (Figures 1D and S2). We stimulated five different spines sequentially by applying the NSP-Uni pattern at each spine first, followed by the NSP-Beg pattern at those spines with the same order, and finally by delivering the NSP-End pattern. After we confirmed that each uncaging pulse can effectively be detected by the spines with each of these defined patterns (NSP-Uni, NSP-Beg, NSP-End), as well as with the 30-Reg LTP paradigm (Figure 1B), we utilized two-photon mediated glutamate uncaging and imaging to induce plasticity at individual spines (Figure 1B-bottom and 1C) and quantified the resulting structural changes before, during and after glutamate delivery (Figures 2 and S3). We first tested whether the homogeneously distributed Poisson pattern (NSP-Uni) was capable of inducing structural plasticity at single inputs. We found that indeed, stimulation with the NSP-Uni pattern led to long-lasting growth of individual spines ($\Delta V_{NSP\text{-}Uni} = 154 \pm 13\%$, Mean $\pm$ SEM, $p = 0.0007$, averaged over the last 45 min window, stimulated versus unstimulated neighbors, Mann-Whitney U) (Figures 2C, 2D, and S4). The amount of growth observed with the NSP-Uni stimulation was similar to that induced with the 30-Reg pattern, consistent with our previous findings ($\Delta V_{30\text{-}Reg} = 172 \pm 9\%$, $p = 0.0003$; $p_{30Reg\text{-}vs\text{-}NSPUni} = 0.1932$). In stark contrast, neither the NSP-Beg ($\Delta V_{NSP\text{-}Beg} = 103 \pm 05\%$, $p = 0.9515$) nor the NSP-End patterns ($\Delta V_{NSP\text{-}End} = 111 \pm 010\%$, $p = 0.5308$) induced long-lasting structural plasticity, with the initial spine growth returning to baseline after approximately 60–75 min (Figure 2C). Importantly, the amount of structural plasticity expressed within the first 15 min after stimulation was not significantly different across the four paradigms

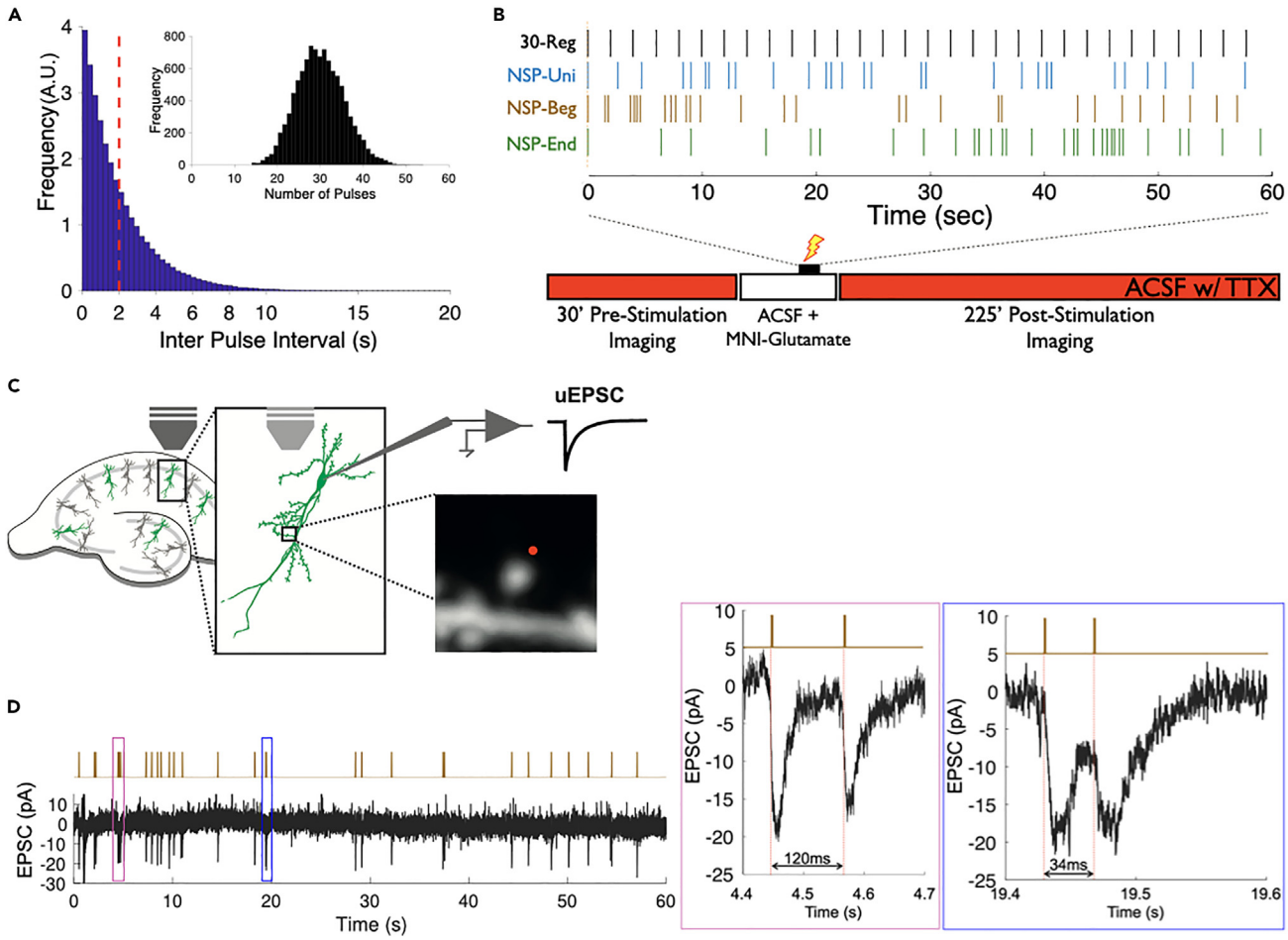

Figure 1. Generation and delivery of naturalistic stimulation patterns at single dendritic spines

(A) Artificially generated Poisson patterns with a λ = 30 and the respective InterPulse Interval distributions (IPI) used to simulate naturalistic activity. The dashed red line represents the average IPI interval of the distribution, which is also the IPI for the 30-Reg pattern (2s). Only 740 out of 10000 generated patterns had exactly 30 events in 60s (inset).

(B) Schematic representation of the experimental flow. Four glutamate uncaging patterns were used in the study. Thin bars (30 total per paradigm) represent pulses within each stimulation pattern, and all pulses are delivered within 60 s. The 30-Reg (Black) pattern has 30 pulses in 60s with a fixed IPI of 2s. The remaining three patterns were picked from among the 740 generated patterns that contained exactly 30 events. Patterns were sorted according to the distribution of events across three 20s time bins: NSP-Uni (Blue) has 10 pulses every 20s, NSP-Beg (Brown) has 15 pulses in the first 20s bin and 15 pulses over the last two time bins spanning 40s, and NSP-End (Green) has 15 pulses within the first two time bins over 40s and 15 pulses in last 20s time bin. Each pattern was delivered in 60 s to a single spine via 2-photon uncaging of MNI-glutamate in ACSF containing 0 mM Mg^{2+} that was introduced via a re-circulation system. Z-stacks of the dendritic branch of interest were imaged every 5 min before stimulation (30 minbaseline) and continued after for approximately 210 min post-stimulation.

(C) Mouse organotypic hippocampal slice cultures were transfected by a gene gun to sparsely label CA1 pyramidal neurons with GFP, and fluorescent neurons were imaged using 2-photon microscopy.

(D) In some experiments, neurons were filled with Alexa dye (0.025 mM Alexa 594) during whole-cell patch-clamp recordings at the cell soma to visualize spines for uncaging and to monitor synaptic responses during uncaging stimuli. The temporal efficacy of responses to individual glutamate uncaging pulses was confirmed with simultaneous uncaging and whole-cell patch-clamp recordings. A representative example from an experiment in which the NSP-Beg pattern was used to stimulate a spine. Pink and blue boxes indicate regions expanded on the right, showing that individual synaptic events that are delivered at either 120 ms or 34 ms respectively, can be detected as separate synaptic events.

(pairwise comparisons averaged over the first 15 min and last 45 min, Figure 2D), indicating that the differences in long-lasting structural plasticity are unlikely because of a stimulation failure.

Given that we observed this for all of the NSPs, we concluded that the lack of long-term structural plasticity following NSP-Beg and NSP-End was not likely because of a reduced number of events detected by the synapse. Even though each activity paradigm contained 30 pulses and was delivered within 60s, only the

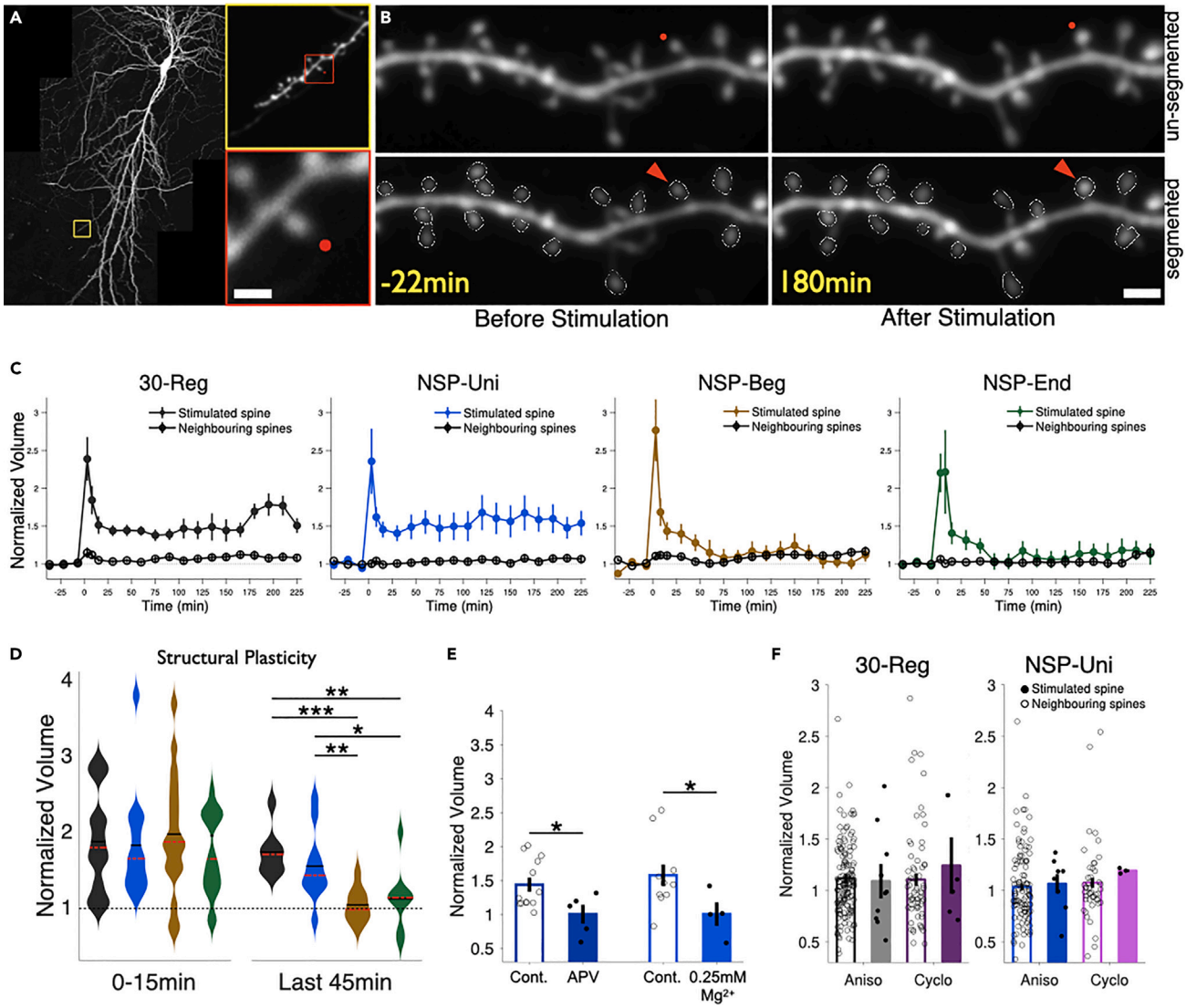

Figure 2. The temporal distribution of uncaging patterns determines the longevity of single-spine plasticity

(A) A 2-photon image of a biolistically transfected CA1 pyramidal neuron in which a single spine undergoes uncaging-mediated stimulation. The red dot represents the uncaging point (720 nm 2-photon laser). The yellow box represents the dendritic region of interest (ROI) that was imaged, and the red box represents a zoomed-in view of the stimulated spine ROI. The scale bar is 2 μm.

(B) A representative uncaging experiment. The upper panel shows the stimulated spine (red dot) and neighboring spines before (left) and after (right) uncaging stimulation. The lower panel shows the same region as above (with the stimulated spine indicated by a red triangle) after the automatic segmentation of spine heads using the SpineS toolbox for volume quantification. The spine was stimulated at time 0 min. The scale bar is 2 μm.

(C) Spine volume changes over 2 h in response to glutamate uncaging-mediated stimulation with different patterns of activity as indicated. Spine volumes are quantified for stimulated and neighboring spine volumes during all four stimulation conditions and are represented as mean ± SEM. The 30-Reg pattern (in black) induced structural plasticity that lasted 3.5 h (n_{stim} = 14, n_{neigh} = 176, N = 11 animals). NSP-Uni (in blue) induced long-lasting plasticity that was similar to the 30-Reg pattern (n_{stim} = 13, n_{neigh} = 155, N = 8 animals). NSP-Beg (in brown) induced only short-lasting changes (n_{stim} = 17, n_{neigh} = 202, N = 8 animals). NSP-End (in green) induced short-lasting structural changes (n_{stim} = 18, n_{neigh} = 264, N = 9 animals). n represents the number of neurons each from an independent slice, whereas N is the number of animals.

(D) All patterns induce structural plasticity within the first minutes following stimulation, however, those induced by NSP-Beg and NSP-End were not long-lasting, and returned to baseline by 60 min post-stimulation ($\Delta V_{NSP\text{-}Uni}$=154±13%, p=0.0007; $\Delta V_{30\text{-}Reg}$=172±9%, p=0.0003; $\Delta V_{NSP\text{-}Beg}$=103±05%, p=0.9515; $\Delta V_{NSP\text{-}End}$=111±010%, p=0.5308. Last 45') (Mann-Whitney U). The average volume change observed during the first 15 min as well as the last 45 min is compared across stimulation paradigms.

Figure 2. *Continued*

(E) NSP-Uni mediated structural plasticity requires NMDA receptor activation and is inhibited with either pharmacological blockade of NMDA receptors using APV or with partial magnesium blockade of those receptors (0.25 mM Mg) (APV: n_{stim} = 5, n_{neigh} = 73; Mg: n_{stim} = 4, n_{neigh} = 44) ($\Delta V_{NSP\text{-}Uni\text{-}APV}$=100±14%, p=0.8224; $\Delta V_{NSP\text{-}Uni\text{-}Mg}$=101±17%, p=0.8040).

(F) The late phase of NSP-Uni-induced structural plasticity is protein synthesis-dependent. Open bars represent neighboring spine volumes, whereas solid bars represent the volume of the stimulated spines. Stimulated spines did not grow in response to activity in the presence of anisomycin or cycloheximide ($\Delta V_{30\text{-}Reg\text{-}ANI}$=109±15%, p=0.6695; $\Delta V_{30\text{-}Reg\text{-}CHX}$=124±22%, p=0.6125; $\Delta V_{NSP\text{-}Uni\text{-}ANI}$=107±9.3%, p=0.4990; $\Delta V_{NSP\text{-}Uni\text{-}CHX}$=119±1%, p=0.1476). Bars represent mean ± SEM (30-Reg: Aniso: n_{stim} = 10, n_{neigh} = 169; Cyclo: n_{stim} = 6, n_{neigh} = 85; $p_{ani\_vs\_cyc}$ = 0.6354. NSP-Uni: Aniso: n_{stim} = 9, n_{neigh} = 126; Cyclo: n_{stim} = 5, n_{neigh} = 72; $p_{ani\_vs\_cyc}$ = 0.4970, unstimulated controls versus stimulated spines, average over last 45', Mann-Whitney U).

30-Reg and NSP-Uni patterns induced significant and long-lasting structural plasticity. These data suggest that the differences in the temporal structures of the stimulation patterns directly contribute to the induction of long-lasting structural plasticity.

Structural plasticity induced by a naturalistic pattern (NSP-Uni) is NMDAR dependent and requires protein synthesis

The regular stimulation of a spine by glutamate uncaging has previously been shown to induce NMDAR-dependent LTP.[1,8] To determine whether plasticity induced by a naturalistic pattern also requires the activation of NMDA receptors, we stimulated spines with the NSP-Uni pattern in the presence of a selective NMDAR antagonist, (2R)-amino-5-phosphonopentanoate (APV), in the uncaging solution (Figure 2E). We found that this manipulation blocked the induction of plasticity, eliciting only a transient potentiation that was not significantly different from baseline ($\Delta V_{NSP\text{-}Uni\text{-}APV}$ = 100 ± 14%, p = 0.8224, averaged over the last 15 min, Figure S5A) and significantly lower than spines stimulated in the absence of APV (p = 0.038, compared to no APV NSP-Uni stimulation) (Figure 2E). To recruit NMDA receptor function, all of the uncaging experiments described thus far were conducted in the absence of extracellular Mg^{2+}, rather than by depolarization via whole-cell patch clamping, because the latter would lead to washout of plasticity-related proteins required for long-term changes.[28] To further validate the requirement for NMDA receptor activation by the NSP-Uni pattern, we also conducted experiments in which we stimulated spines in the presence of 0.25 mM extracellular Mg^{2+}. This partial blockade of NMDARs prevented structural plasticity in response to glutamate uncaging ($\Delta V_{NSP\text{-}Uni\text{-}Mg}$ = 101 ± 17%, p = 0.8040, average of the last 45 min) (Figures 2E and S5B), and was significantly lower than that observed with control conditions (p = 0.0223, compared to 0 mM Mg^{2+}) (Figure 2E).

Long-lasting functional plasticity that induces new protein synthesis leads to long-lasting structural changes.[8] As we observed that the plasticity elicited at single spines with the NSP-Uni pattern led to structural changes that lasted for many hours, we hypothesized that this process is also protein synthesis-dependent, like its regular counterpart. Therefore, we performed both the 30-Reg and NSP-Uni stimulations in the presence of protein synthesis inhibitors, either anisomycin (ANI) or cycloheximide (CHX), and evaluated the resulting changes. We confirmed that the late-phase of structural plasticity was abolished when protein synthesis was inhibited during the induction of plasticity with the Regular pattern ($\Delta V_{30\text{-}Reg\text{-}ANI}$ = 109 ± 15%, p = 0.6695, average of the last 45 min, compared to unstimulated controls; $\Delta V_{30\text{-}Reg\text{-}CHX}$ = 124 ± 22%, p = 0.6125) (Figures 2F left panel, S5C, and S5D left panels), in agreement with previous observations.[28] We found that a similar blockade of structural plasticity was induced when the naturalistic pattern NSP-Uni was delivered in the presence of protein synthesis inhibitors, irrespective of the drug utilized ($\Delta V_{NSP\text{-}Uni\text{-}ANI}$ = 107 ± 9.3%, p = 0.4990; $\Delta V_{NSP\text{-}Uni\text{-}CHX}$ = 119 ± 1%, p = 0.1476) (Figures 2F right, S5C, and S5D right panels). Thus, we find that the structural plasticity that is induced by a naturalistic pattern (NSP-Uni) at a single input is both NMDAR and protein synthesis-dependent, matching the qualities of functional and structural plasticity that have been previously described.

Rapid spine growth during naturalistic stimulation predicts the longevity of the resulting structural plasticity

During the induction of glutamate uncaging-mediated plasticity, a rapid initial increase in spine volume occurs.[1,7,28] We wanted to determine whether similar rapid changes are triggered during naturalistic patterns of activity at individual spines. To visualize the temporal dynamics of spine growth that occurs during stimulation, we collected two-photon images of dendritic spines during the 60s period of glutamate uncaging for each paradigm. We tracked the growth of individual spines during this 60s stimulation period (Figure 3A) and quantified the area under the curve to determine volume changes (see Figure S7). We found

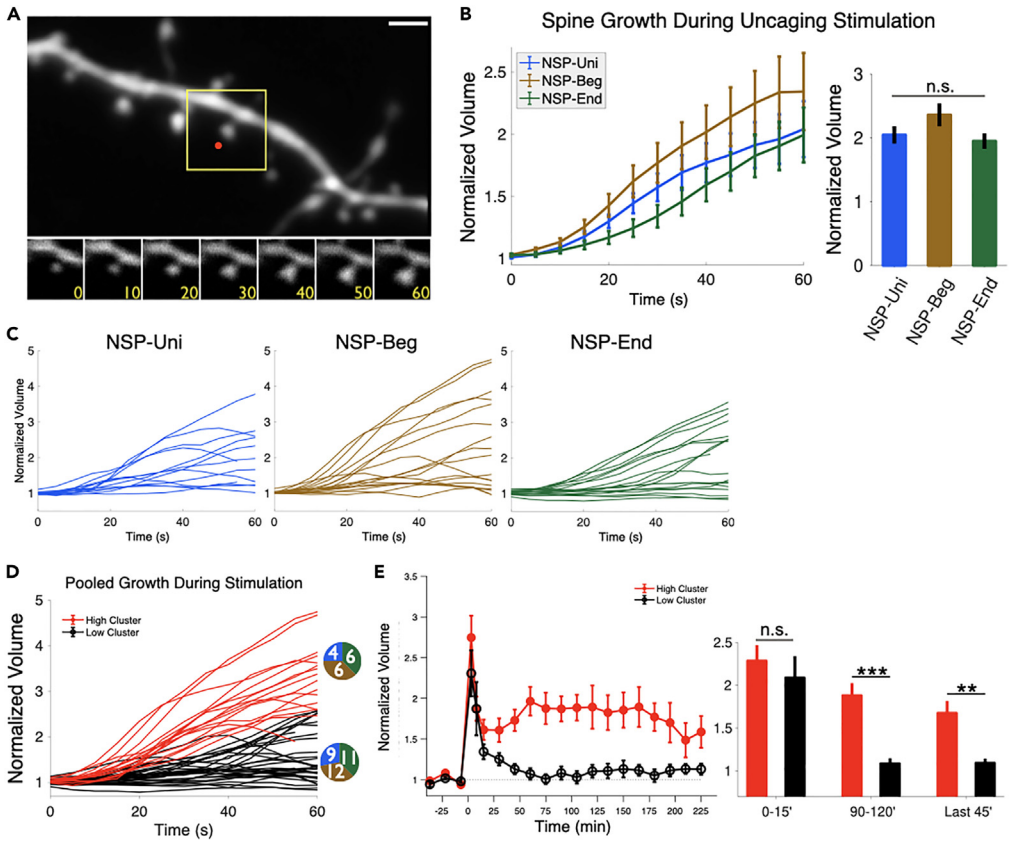

Figure 3. Rapid spine growth during the stimulation predicts the longevity of structural plasticity induced by naturalistic patterns

(A) Rapid structural growth is observed during the 60 s of glutamate uncaging-mediated stimulation. The upper panel shows the dendrite of interest and the stimulated spine is contained within the yellow box (indicated by a red dot). The lower panels show spine structural growth over the course of the stimulation (in seconds). The scale bar is 2 μm.

(B) Statistical comparison of the average growth data during each stimulation condition reveals no difference between the naturalistic patterns ($\Delta V_{30\text{-}Reg}$=226±37%; $\Delta V_{NSP\text{-}Uni}$=190±19%; $\Delta V_{NSP\text{-}Beg}$=195±19:8%; $\Delta V_{NSP\text{-}End}$=236±37%. p=0.7806, repeated-measures ANOVA with lower-bound adjustment).

(C) Rapid growth dynamic trajectories for all of the individual spines stimulated with the respective NSP pattern: Uni, Beg, End (Blue, Brown, and Green)($n_{NSP\text{-}Uni}$ = 13, $n_{NSP\text{-}Beg}$ = 17, $n_{NSP\text{-}End}$ = 18, n_{High} = 16,n_{Low} = 32).

(D) Pooled growth curves from each of the three NSP patterns. Rapid growth curves were divided into two classes using a k-means algorithm and color-coded accordingly (*High* growers: red, *Low* growers black). Numbers in the adjacent pie charts show the contribution of each condition to that particular cluster.

(E) Long-term spine volume changes were plotted according to the k-means identified grouping of high (red) or low growers (black), demonstrating correspondence between the rapid structural changes and the long-lasting ones. This is quantified in the bar graphs on the right, showing that although both clusters induced similar levels of initial structural plasticity (at 15′), the longevity of plasticity significantly diverges, as seen at time bins around 100′ and 225′ ($p_{0\text{-}15'}$ = 0.0646, $p_{90\text{-}120'}$ = 7.9883e-4, $p_{180\text{-}225'}$ = 0.0086, Mann-Whitney U).

that on average, all four stimulation conditions (30-Reg, NSP-Uni, NSP-Beg, NSP-End) induced similar levels of structural plasticity during the 60-s stimulation ($\Delta V_{30\text{-}Reg}$ = 226 ± 37%; $\Delta V_{NSP\text{-}Uni}$ = 190 ± 19%; $\Delta V_{NSP\text{-}Beg}$ = 195 ± 19:8%; $\Delta V_{NSP\text{-}End}$ = 236 ± 37%, at 60s) (Figure 3B) that were not significantly different from each other (p = 0.7806, repeated-measures ANOVA with lower-bound adjustment, Figure 3B).

We noticed that there was a considerable degree of variability in the amount of structural plasticity expressed by different spines during the stimulation, with some spines showing low volume changes compared to others that grew considerably, even in response to the same stimulation pattern (Figure 3C). We wondered whether these differences in short-term dynamics could be predictive of long-term structural plasticity outcomes of individual spines. As our three naturalistic paradigms (NSP-Uni, NSP-Beg, NSP-End)

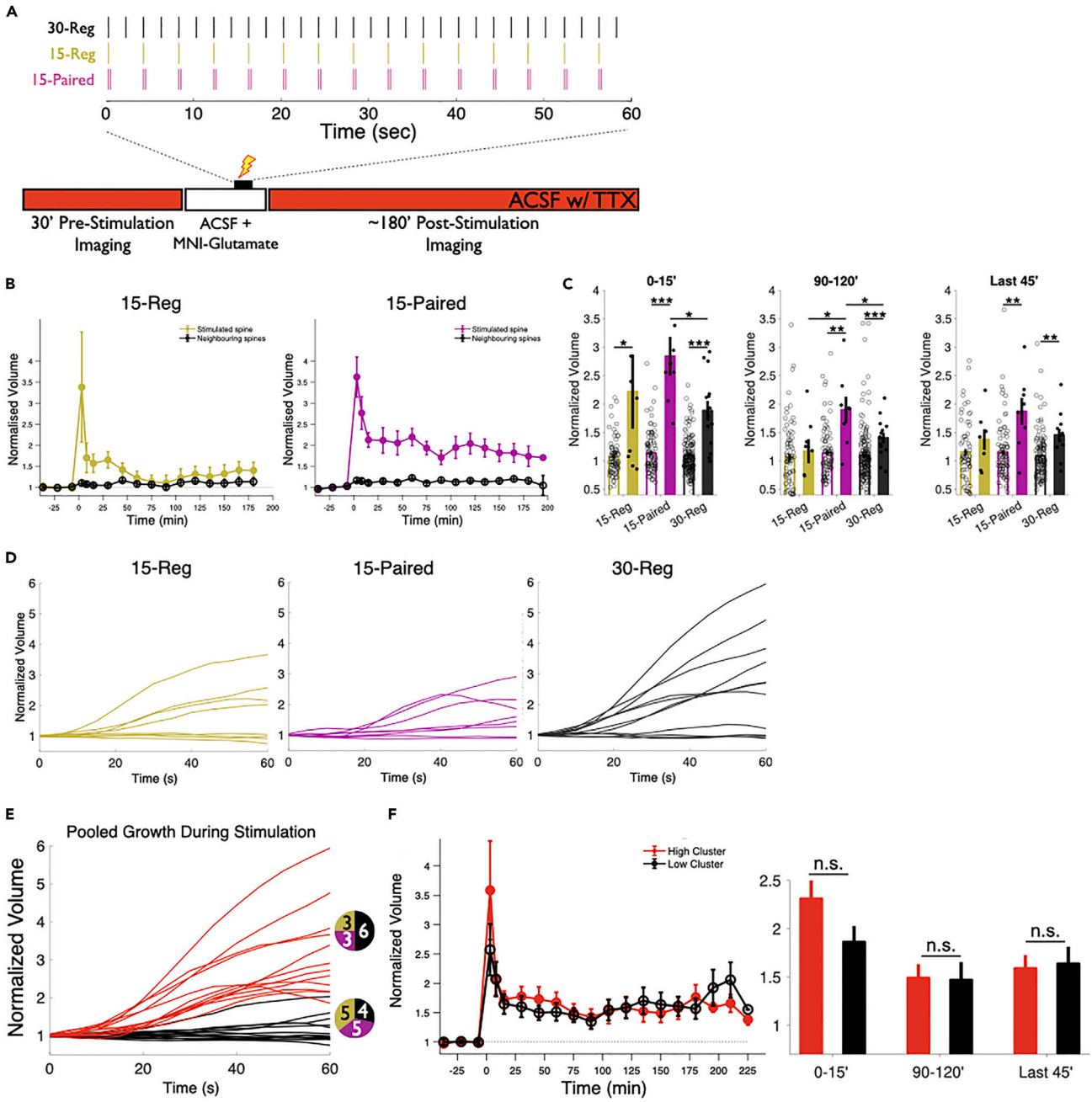

Figure 4. Rapid spine growth with stationary uncaging patterns does not predict the longevity of structural plasticity

(A) Schematic of the stationary stimulation patterns used to induce structural plasticity at single spines. In addition to the 30-Reg (black) pattern (30 pulses at 0.5 Hz), we also tested a pattern that delivered half the number of pulses at the same time (15-Reg, 0.25 Hz, yellow) and a pattern that delivered the same 30 pulses in the form of 15 pairs with a 50 ms inter-pulse-interval (15-Paired, magenta).

(B) Spine structural plasticity as measured by volume increases following stimulation with either the 15-Reg (yellow) pattern or the 15-Paired (magenta) pattern. The 15-Reg pattern shows only short-term structural changes, whereas the 15-Paired stimulation produces robust long-lasting structural plasticity.

(C) The 15-Paired pattern (magenta) induced long-lasting structural changes whereas the 15-Reg pattern (yellow) only gave rise to short-term structural changes. The 15-Paired stimulation induced higher levels of structural plasticity in spines during the first 120′ even when compared to the 30-Reg pattern. Spine volumes were quantified and averaged across three different time bins after stimulation: 0–15′, 90–120′, and the last 45′. Comparisons between average values in these bins were made between corresponding unstimulated neighbors and between conditions, using Mann-Whitney U. Solid bars represent spine growth at the indicated time bin, and open bars represent spine volume changes at the unstimulated neighbors. P-values are as follows: **0–15′**: 15-Reg (stim v neighbors, p = 0.032), 15-Paired (stim v neighbors p = 5.7083e-6), 30-Reg (stim v neighbors, p = 2.55e-6), **15-Paired v 30-Reg** (p = 0.265); **90–120′**: 15-Reg (stim v neighbors, p = 0.5671), 15-Paired (stim v neighbors p = 0.0014), 30-Reg (stim v neighbors, p = 7.2826e-4), **15-Reg v 15-Paired**

Figure 4. *Continued*

(p = 0.0379), **15-Reg v 30-Reg** (p = 0.2067); **last 45'**: 15-Reg (stim v neighbors, p = 0.2844), 15-Paired (stim v neighbors p = 0.0027), 30-Reg (stim v neighbors, p = 0.0023), **15-Reg v 15-Paired** (**p=0.1893**); **15-Paired v 30-Reg** (p = 0.1288).

(D) Rapid growth dynamics during the stimulation with either the 15-Reg, 15-Paired, or 30-Reg stimulations show that individual spines exhibit variable amounts of growth during the stimulation similar to what we observed during the NSP stimulations.

(E) Rapid spine growth trajectories during the stimulations of 30-Reg, 15-Reg, and 15-Paired ($n_{15\text{-}Reg}$ = 8, $n_{15\text{-}Paired}$ = 8, $n_{30\text{-}Reg}$ = 10) were pooled. Numbers in the adjacent pie charts show the relative contribution per condition from each stimulation group, obtained by k-means cluster analysis.

(F) Short-term structural plasticity groups were evaluated for their correlation with long-term structural outcomes and graphed according to the rapid growth clusters identified by k-means analysis. Both groups induced equal amounts of structural plasticity ($p_{0\text{-}15'}$ = 0.6597, $p_{90\text{-}120'}$ = 0.9805, $p_{180\text{-}225'}$ = 1, Mann-Whitney U).

came from the same distribution, we pooled their rapid growth dynamics and clustered them into two groups using a k-means algorithm[29] (Figure 3D). The obtained clusters were termed *High* and *Low*, reflecting differences in total growth during the initial 60s of stimulus delivery. Accordingly, we plotted the corresponding long-term volume changes based on these clusters (Figure 3E left panel and individually in Figure S6). We found that spines that grew more during the stimulation (in the *High* cluster) exhibited long-lasting structural plasticity (ΔV_{High} = 158 $\pm$ 20%, average of last 45 min), whereas spines that showed little growth (in the *Low* cluster) exhibited only short-lived volume changes (ΔV_{Low} = 113 $\pm$ 7%, Figure 3E right panel and Figure S6). We also found that a second analysis, in which the data were fit to a bimodal Gaussian distribution, showed similar results in which two groups of low and high growers predicted which spines underwent long-term structural changes based on their rapid growth dynamics (Figure S7).

It has previously been shown that it is easier to induce plasticity at smaller dendritic spines.[1] However, if the stimulus is sufficiently strong, plasticity can be elicited across spines of different sizes.[8,26,30,31] To see whether differences in High and Low clusters correlate with differences in initial spine sizes, we checked the distribution of the initial spine size for spines within each of the Low and High growing clusters for each stimulation pattern. We did not observe any significant correlations between initial spine size and the extent of spine growth (Figure S8).

Therefore, although different activity patterns led to clear differences in long-term structural plasticity, the short-term dynamics revealed that a higher diversity of responses existed among the population of individual spines to these stimuli. Furthermore, we found that the degree to which any given spine grows over the course of naturalistic activity is highly predictive of the structural plasticity that it will subsequently express.

The longevity of structural plasticity also varies with more regular temporal patterns, yet is not correlated with short-term spine dynamics

We wondered what aspect of the pulse distribution among the different protocols was leading to the differences in the longevity of structural plasticity that were elicited. We considered the possibility that the consistent delivery of stimuli over the entirety of the 60s window, rather than the number of stimuli per se, was the critical parameter to the induction of long lasting plasticity. In addition, it was unknown whether the closely spaced stimuli that occurred at various intervals in the NSPs would contribute to the induction of plasticity with the same efficacy as events that are more evenly distributed during the activity pattern. To test these possibilities, we designed two alternative stimulation patterns (15-Reg and 15-Paired) that were stationary in nature and that would be delivered over the same 60s period as our 30 pulse protocol (30-Reg, Figure 4A).

We first stimulated individual spines with a lower frequency stimulation that was nevertheless regular in nature, by delivering 15 equally spaced pulses (15-Reg: at 0.25Hz). The 15-Reg pattern only induced weak growth, which by 60-75min after the stimulation was not significantly different from baseline ($\Delta V_{15\text{-}Reg}$ = 137 $\pm$ 15%, p = 0.2844, average over the last 45min, compared to neighbors) (Figure 4B). This is similar to the length for which structural changes lasted with both NSP-Beg and NSP-End. This finding indicates that a regular pattern of stimulation alone is not sufficient to induce long-lasting structural plasticity.

We next wanted to determine if the inter-pulse-interval impacted the induction of structural plasticity, as this varied in our NSP paradigms. We delivered 15 pairs of pulses (15-Paired: 15 pairs of pulses spaced 50 ms apart, delivering a total of 30 pulses at 0.5Hz) to test whether 30 stimulations, in which half occurred in closely spaced temporal proximity to one another (50 ms), would give rise to structural plasticity of similar

magnitude to that induced with evenly distributed events. We found that the 15-Paired protocol produced long-lasting structural plasticity ($\Delta V_{15\text{-paired}}$ =187 ± 23%, p = 0.0027, average of the last 45 min, compared to neighbors) (Figure 4C left panel) that was similar in magnitude to what we observed with the 30-Reg paradigm (p = 0.6126, average of the last 45min) (Figure 4C right panel). The fact that the 15-Paired protocol yielded long-lasting structural plasticity while the 15-Reg did not, suggests that each pulse likely contributes toward the induction of plasticity and that the close temporal proximity of the pulses does not compromise their salience, in accordance with our initial observations (Figure 1D). Indeed, our findings show that stimulation with 30 pulses delivered as pairs (15-Paired) induces a greater amount of structural plasticity in the first 15 min compared to one in which the pulses are distributed regularly (30-Reg), suggesting that this paradigm may be more efficient at inducing structural plasticity (p = 0.0265, average of the first 15min, Figure 4C left panel). Together, these data indicate that a minimal quantity of stimulation is required to achieve long-lasting structural plasticity and that the regularity of a pattern, in and of itself, is insufficient to accomplish this.

As we had observed variability in the amount of spine volume growth during the stimulations with naturalistic patterns, we wondered whether similar spine growth dynamics would be observed during the delivery of the stationary paradigms (30-Reg, 15-Reg, 15-Paired) (Figure 4D). Therefore, we tested whether short-term volume changes were predictive of long-term structural plasticity outcomes. Spines stimulated with regular stimulation patterns did indeed produce a range of responses and we classified them into *Low* and *High* growing groups, as with spines following NSP stimulations (Figures 4D and 4E). However, unlike the case of NSPs, *Low* and *High* growing spine group responses during stationary patterns of activity did not correlate with divergent long-term structural outcomes but instead showed equivalent amounts of long term growth (ΔV_{Low} = 163 ± 18%, ΔV_{High} = 159 ± 14%, p = 0.7618, average of the last 45 min) (Figures 4F and S9). This observation is in stark contrast with the naturalistic paradigms whose short-term spine dynamics predicted the longevity of plasticity.

DISCUSSION

How neurons and synapses respond to the diverse patterns of activity that they receive, and how they change to permit the long-term storage of that experience, remains a fundamental question that is yet to be understood in neuroscience. Synaptic plasticity has been widely studied through the delivery of regular trains of activity, but these have much less often reproduced the irregularities of inter-spike intervals that are common during endogenous activity.[16,32,33] Whether such irregular patterns can induce plasticity at single inputs and what if any would be the structural consequences of this form of activity has not been explored. Here, using two-photon fluorescence imaging and glutamate uncaging, we studied single spine structural plasticity of CA1 pyramidal neurons using stimulation patterns sampled from a Poisson process, resembling firing patterns of CA3 neurons. For the first time, we have shown that the longevity of this plasticity is determined by the temporal structure of NSPs. In addition, we demonstrate that rapid structural changes induced by NSPs, but not by stationary patterns, predict the longevity of the induced changes. These findings suggest that a single dendritic spine has the capacity to integrate temporal information with millisecond resolution and that the result of this transformation can modulate the longevity of plasticity that is expressed. Furthermore, the rapid growth of the spine in response to stimuli can predict whether that activity was sufficiently salient to induce long-term structural plasticity.

In our experiments, NSP-Uni was the only naturalistic pattern that induced long-lasting structural changes. This finding was surprising, given that each of the naturalistic activity patterns delivered the same total amount of glutamate over the same period to each spine (30 pulses over 60s). Nevertheless, the pattern of activity delivered in that first minute influenced the structural plasticity that was expressed over subsequent hours. What is the critical difference between these? Although sampled from the same Poisson distribution, NSP-Beg and NSP-End had instantaneous frequencies over time that were considerably different from NSP-Uni, which was the only pattern to induce long-lasting plasticity and was the most similar in the distribution of events to that of the 30-Reg pattern (see Figure S2). These time-frequency structures may influence Ca^{2+} concentrations and thus impact the signaling pathways that are recruited during the induction of plasticity.[34] This is further evidenced by the robust plasticity induced by the 15-Paired train, in which the 30 pulses are delivered in pairs of 50 ms stimuli. When delivered electrically, such pulses are known to activate mGluRs and induce protein synthesis-dependent plasticity that is long-lasting.[35] We indeed observe these spacings in our naturalistic protocols (Figures S1 and S10), and it will be interesting to determine in future studies to what extent these events contribute to the robustness of LTP and what is the

minimum frequency of such pairs that may be required to induce plasticity. Therefore, stationarity seems to be an important component that leads to the induction of long-lasting structural plasticity, even though it may not be sufficient to induce plasticity if a minimum stimulation threshold is not achieved. We find that with half the number of stimulations of our standard protocol (15-Reg), regularity itself is not sufficient to induce plasticity (Figure 4B). This is in agreement with previous findings in which 1 ms-long, rather than 4 ms-long, uncaging pulses do not induce structural changes.[7,8]

It had previously been shown that dendritic spine structure can change rapidly on activation.[23,36–38] When we examined the rapid structural responses of spines during different stimulation paradigms, we did not see significant differences between their responses to the four different conditions. However, when we investigated individual structural growth traces, we noticed variability across spines. Clustering analyses revealed that the relationship between short- and long-term dynamics is stimulation pattern-dependent for naturalistic patterns. On the other hand, no such relationship was observed with regular patterns of activity. These findings suggest that there is a difference in the saliency of the naturalistic patterns compared to that of stationary activity at individual spines, and it will be important to identify what are the critical features of non-stationary patterns of activity and the inputs that they engage, which gives rise to such variabilities in structural plasticity outcomes. Furthermore, how these short-term temporal dynamics engage downstream signaling processes, such as protein-synthesis-dependent mechanisms, remains to be determined.

We found that NSP-Uni requires NMDA-R activation and new protein synthesis, thereby utilizing the canonical pathways involved in the induction and maintenance of synaptic functional and structural plasticity. Importantly, our findings demonstrate that synaptic activity patterns can differentially induce long-lasting and protein synthesis-dependent structural plasticity. The late phase of LTP as well as long-lasting structural plasticity with regular patterns requires newly synthesized proteins.[8,39,40] Our results demonstrate that naturalistic patterns of activity induce similar mechanisms at individual spines, and it will be important to determine what are the temporal dynamics of the signaling targets which regulate the function of these critical plasticity pathways.

One consequence of activity through NMDARs, necessary for the induction of functional and structural plasticity, is postsynaptic calcium entry. Differential concentrations of Ca^{2+} have been proposed as mechanisms for establishing bidirectional changes in plasticity, via distinct activation of kinase or phosphatase-driven pathways.[34,41–43] It will be important to examine whether alternative NSP patterns can induce bidirectional forms of structural plasticity. In addition, the temporal microdomains within the naturalistic patterns could dynamically modulate the relative balance of active signaling components necessary for determining the direction of structural plasticity. Future efforts to define these microdomains and characterize which pathways they activate will be essential to understanding the activity code which drives synaptic changes.

Another potential effect of such activity microdomains could be that they differentially give rise to short-term facilitation or depression, which in turn may overlap with subsequent signaling pathways as they are being induced. Activity patterns may effectively give rise to synaptic integration of plasticity at the level of a single input. A stimulation protocol that only activates one pathway would not lead to such interactions. Furthermore, the regularity of the pattern may itself induce a more salient form of plasticity that overrides any pre-existing outputs of a synapse. This may explain why the rapid dynamics that followed naturalistic patterns predicted long-lasting structural plasticity, whereas the ones induced by the regular patterns did not.

Several molecular players may serve as key integrators of plasticity and could report the temporal structure of naturalistic patterns. A recent computational study predicts the synergistic activation of the extracellular signal-regulated kinase (ERK) pathway in a temporally dependent manner through the convergence of calcium signals with cAMP activation.[44] The model accounts for differences in the extent of pathway activation based on either the total activity delivered or the rate of peak activity. Further evidence supporting a role for calcium as an integrator of instantaneous frequencies comes from a computational model of spiny projection neurons in the striatum. Here, a calcium-based plasticity rule could determine the direction of plasticity as the amplitudes and duration thresholds of spine calcium concentrations vary.[45] Thus, fluctuations in the amount of postsynaptic calcium during an NSP could lead to the convergence of several signaling events. Another protein that is crucial for the induction of LTP, Calcium/calmodulin kinase II (CaMKII), is regulated in an activity-dependent manner at its subunits that are sensitive to the overall number and frequency of stimuli.[38,46,47] Blocking the autophosphorylation of a key regulatory site on CaMKIIα at Thr286

during stimulation impairs the long-term growth of spines; an effect that can be overcome by increasing the frequency and number of pulses.[48] This suggests that different temporal patterns of activity may vary in their ability to initiate signaling through CamKIIα or one of its key effectors, such as the Rho GTPase Cdc42, whose short activation period and spatial restriction to spines are required for structural plasticity.[49] Thus, the patterns of activity delivered by our NSP protocols may differentially activate, or fail to activate key synaptic components. NSPs might recruit kinases or phosphatases, depending on the extent of post-synaptic calcium that arises because of their instantaneous-frequency fluctuations. It will be important to evaluate the calcium signals that are generated at single spines during stimulation with these patterns and to correlate these with the requirements for the activation of different kinases.

Here, we present the first experimental evidence demonstrating that the temporal organization of Poisson-based activity affects differential long-lasting structural plasticity at individual inputs. The structural modifications that are induced by these naturalistic patterns act through canonical plasticity mechanisms, recruiting NMDA receptor function and inducing new protein synthesis. Of interest, we observed that as individual spines experienced activity, they underwent rapid and diverse structural changes that were predictive of their subsequent long-term structural changes. These findings begin to elucidate the learning rules for encoding naturalistic activity patterns into long-lasting physical modifications of spines, the fundamental inputs of neuronal activity.

Limitations of the study

The correlation between the physical structure of a dendritic spine such as volume and the amount of current it conducts is well established.[1,3,7,8] This suggests that changes in spine volume can serve as a useful proxy for measuring alterations in functional plasticity. Here we utilized the same approach to measure the level of plasticity caused by different stimulation patterns. However, it cannot be ruled out that certain physiological changes induced by naturalistic patterns may manifest themselves in different structural states. It would be interesting to observe how a dendritic spine's structural and functional properties are coupled in response to naturalistic patterns. In addition, we have only used a subset of naturalistic patterns in our experiments. It would be fascinating to try the rest of the patterns to create a complete mapping of the timing structure and plasticity relationships. This is an area of interest for future research.

STAR★METHODS

Detailed methods are provided in the online version of this paper and include the following:

- KEY RESOURCES TABLE
- RESOURCE AVAILABILITY
  - Lead contact
  - Materials availability
  - Data and code availability
- EXPERIMENTAL MODEL AND SUBJECT DETAILS
  - Experimental animals
- METHOD DETAILS
  - Preparation of organotypic slice cultures
  - Biolistic gene transfection
  - Patch clamp Electrophysiology
  - Generation of naturalistic stimulation patterns
  - Two-photon imaging and uncaging
- QUANTIFICATION AND STATISTICAL ANALYSIS

SUPPLEMENTAL INFORMATION

Supplemental information can be found online at https://doi.org/10.1016/j.isci.2023.106835.

ACKNOWLEDGMENTS

We thank members of the Israely Lab, specifically Anna F. Hobbiss and Yazmin R. Cortes for their technical support throughout the study and Ana Vaz for help with animal care. We also thank Yazmin R. Cortes, Nicolas A. Morgenstern, Daniela Pereira, Tevye J. Stachniak, Martin Müller, and Theofanis Karayannis for critical reading of the manuscript and feedback. We thank Gil Costa for the design help with Figure 1C and the

graphical abstract. A.Ö.A. was supported by Fundação para a Ciência e a Tecnologia (FCT) grant SFRH/BD/51264/2010. The study was also supported by grants from the Bial Foundation (161/10-2010), FCT (PTDC/SAU-NMC/122035/2010), and the National Institutes of Health (1R01NS112485) to I.I.

AUTHOR CONTRIBUTIONS

A.Ö.A and I.I. designed the experiments. A.Ö.A performed the experiments, analyzed the data, and drafted the manuscript. I.I. supervised the study and wrote the manuscript.

DECLARATION OF INTERESTS

The authors declare no competing interests.

INCLUSION AND DIVERSITY

We support inclusive, diverse, and equitable conduct of research.

Received: February 18, 2022
Revised: January 18, 2023
Accepted: May 4, 2023
Published: May 8, 2023

REFERENCES

1. Matsuzaki, M., Honkura, N., Ellis-Davies, G.C.R., and Kasai, H. (2004). Structural basis of long-term potentiation in single dendritic spines. Nature *429*, 761–766. https://doi.org/10.1038/nature02617.

2. Malenka, R.C., and Bear, M.F. (2004). LTP and LTD: an embarrassment of riches. Neuron *44*, 5–21. https://doi.org/10.1016/j.neuron.2004.09.012.

3. Bartol, T.M., Jr., Bromer, C., Kinney, J., Chirillo, M.A., Bourne, J.N., Harris, K.M., and Sejnowski, T.J. (2015). Nanoconnectomic upper bound on the variability of synaptic plasticity. Elife *4*, e10778. https://doi.org/10.7554/eLife.10778.

4. Holler, S., Köstinger, G., Martin, K.A.C., Schuhknecht, G.F.P., and Stratford, K.J. (2021). Structure and function of a neocortical synapse. Nature *591*, 111–116. https://doi.org/10.1038/s41586-020-03134-2.

5. Smith, M.A., Ellis-Davies, G.C., and Magee, J.C. (2003). Mechanism of the distance-dependent scaling of Schaffer collateral synapses in rat CA1 pyramidal neurons. J. Physiol. *548*, 245–258. https://doi.org/10.1111/j.1469-7793.2003.00245.x.

6. Losonczy, A., and Magee, J.C. (2006). Integrative properties of radial oblique dendrites in hippocampal CA1 pyramidal neurons. Neuron *50*, 291–307. https://doi.org/10.1016/j.neuron.2006.03.016.

7. Harvey, C.D., and Svoboda, K. (2007). Locally dynamic synaptic learning rules in pyramidal neuron dendrites. Nature *450*, 1195–1200. https://doi.org/10.1038/nature06416.

8. Govindarajan, A., Israely, I., Huang, S.Y., and Tonegawa, S. (2011). The dendritic branch is the preferred integrative unit for protein synthesis-dependent LTP. Neuron *69*, 132–146. https://doi.org/10.1016/j.neuron.2010.12.008.

9. Frey, U., and Morris, R.G. (1997). Synaptic tagging and long-term potentiation. Nature *385*, 533–536. https://doi.org/10.1038/385533a0.

10. McGaugh, J.L. (2000). Memory–a century of consolidation. Science *287*, 248–251. https://doi.org/10.1126/science.287.5451.248.

11. Fonseca, R., Nägerl, U.V., and Bonhoeffer, T. (2006). Neuronal activity determines the protein synthesis dependence of long-term potentiation. Nat. Neurosci. *9*, 478–480. https://doi.org/10.1038/nn1667.

12. Bliss, T.V., and Lømo, T. (1973). Long-lasting potentiation of synaptic transmission in the dentate area of the anaesthetized rabbit following stimulation of the perforant path. J. Physiol. *232*, 331–356. https://doi.org/10.1113/jphysiol.1973.sp010273.

13. Ito, M., and Kano, M. (1982). Long-lasting depression of parallel fiber-Purkinje cell transmission induced by conjunctive stimulation of parallel fibers and climbing fibers in the cerebellar cortex. Neurosci. Lett. *33*, 253–258. https://doi.org/10.1016/0304-3940(82)90380-9.

14. Bear, M.F., and Malenka, R.C. (1994). Synaptic plasticity: LTP and LTD. Curr. Opin. Neurobiol. *4*, 389–399. https://doi.org/10.1016/0959-4388(94)90101-5.

15. Softky, W.R., and Koch, C. (1993). The highly irregular firing of cortical cells is inconsistent with temporal integration of random EPSPs. J. Neurosci. *13*, 334–350. https://doi.org/10.1523/JNEUROSCI.13-01-00334.1993.

16. Dobrunz, L.E., and Stevens, C.F. (1999). Response of hippocampal synapses to natural stimulation patterns. Neuron *22*, 157–166. https://doi.org/10.1016/S0896-6273(00)80687-X.

17. Frerking, M., Schulte, J., Wiebe, S.P., and Stäubli, U. (2005). Spike timing in CA3 pyramidal cells during behavior: implications for synaptic transmission. J. Neurophysiol. *94*, 1528–1540. https://doi.org/10.1152/jn.00108.2005.

18. Chokshi, V., Grier, B.D., Dykman, A., Lantz, C.L., Niebur, E., Quinlan, E.M., and Lee, H.K. (2021). Naturalistic spike trains drive state-dependent homeostatic plasticity in superficial layers of visual cortex. Front. Synaptic Neurosci. *13*, 663282. https://doi.org/10.3389/fnsyn.2021.663282.

19. Mainen, Z.F., and Sejnowski, T.J. (1995). Reliability of spike timing in neocortical neurons. Science *268*, 1503–1506. https://doi.org/10.1126/science.7770778.

20. Vinje, W.E., and Gallant, J.L. (2002). Natural stimulation of the nonclassical receptive field increases information transmission efficiency in V1. J. Neurosci. *22*, 2904–2915. https://doi.org/10.1523/JNEUROSCI.22-07-02904.2002.

21. Faisal, A.A., Selen, L.P.J., and Wolpert, D.M. (2008). Noise in the nervous system. Nat. Rev. Neurosci. *9*, 292–303. https://doi.org/10.1038/nrn2258.

22. Herikstad, R., Baker, J., Lachaux, J.P., Gray, C.M., and Yen, S.C. (2011). Natural movies evoke spike trains with low spike time variability in cat primary visual cortex. J. Neurosci. *31*, 15844–15860. https://doi.org/10.1523/JNEUROSCI.5153-10.2011.

23. Harvey, C.D., Yasuda, R., Zhong, H., and Svoboda, K. (2008). The spread of Ras activity triggered by activation of a single dendritic spine. Science *321*, 136–140. https://doi.org/10.1126/science.115967.

24. Hill, T.C., and Zito, K. (2013). LTP-induced long-term stabilization of individual nascent dendritic spines. J. Neurosci. *33*, 678–686.

https://doi.org/10.1523/JNEUROSCI.1404-12.2013.

25. Bosch, M., Castro, J., Saneyoshi, T., Matsuno, H., Sur, M., and Hayashi, Y. (2014). Structural and molecular remodeling of dendritic spine substructures during long-term potentiation. Neuron *82*, 444–459. https://doi.org/10.1016/j.neuron.2014.03.021.

26. Hobbiss, A.F., Ramiro-Cortés, Y., and Israely, I. (2018). Homeostatic plasticity scales dendritic spine volumes and changes the threshold and specificity of Hebbian plasticity. iScience *8*, 161–174. https://doi.org/10.1016/j.isci.2018.09.015.

27. Rich, P.D., Liaw, H.P., and Lee, A.K. (2014). Large environments reveal the statistical structure governing hippocampal representations. Science *345*, 814–817. https://doi.org/10.1126/science.1255635.

28. Kruijssen, D.L.H., and Wierenga, C.J. (2019). Single synapse LTP: a matter of context? Front. Cell. Neurosci. *13*, 496. https://doi.org/10.3389/fncel.2019.00496.

29. Bishop, C.M. (2006). Pattern recognition and machine learning. Springer *4*, 738. No. 4.

30. Oh, W.C., Hill, T.C., and Zito, K. (2013). Synapse-specific and size-dependent mechanisms of spine structural plasticity accompanying synaptic weakening. Proc. Natl. Acad. Sci. USA *110*, E305–E312. https://doi.org/10.1073/pnas.121470511.

31. Ramiro-Cortés, Y., and Israely, I. (2013). Long lasting protein synthesis-and activity-dependent spine shrinkage and elimination after synaptic depression. PLoS One *8*, e71155. https://doi.org/10.1371/journal.pone.0071155.

32. Zador, A.M., and Dobrunz, L.E. (1997). Dynamic synapses in the cortex. Neuron *19*, 1–4. https://doi.org/10.1016/S0896-6273(00)80341-4.

33. Paulsen, O., and Sejnowski, T.J. (2000). Natural patterns of activity and long-term synaptic plasticity. Curr. Opin. Neurobiol. *10*, 172–179. https://doi.org/10.1016/S0959-4388(00)00076-3.

34. Cooper, L.N., and Bear, M.F. (2012). The BCM theory of synapse modification at 30: interaction of theory with experiment. Nat. Rev. Neurosci. *13*, 798–810. https://doi.org/10.1038/nrn3353.

35. Kemp, N., and Bashir, Z.I. (1999). Induction of LTD in the adult hippocampus by the synaptic activation of AMPA/kainate and metabotropic glutamate receptors. Neuropharmacology *38*, 495–504. https://doi.org/10.1016/S0028-3908(98)00222-6.

36. Van Harreveld, A., and Fifkova, E. (1975). Swelling of dendritic spines in the fascia dentata after stimulation of the perforant fibers as a mechanism of post-tetanic potentiation. Exp. Neurol. *49*, 736–749. https://doi.org/10.1016/0014-4886(75)90055-2.

37. Fifková, E. (1985). A possible mechanism of morphometric changes in dendritic spines induced by stimulation. Cell. Mol. Neurobiol. *5*, 47–63. https://doi.org/10.1007/BF00711085.

38. Lee, S.J.R., Escobedo-Lozoya, Y., Szatmari, E.M., and Yasuda, R. (2009). Activation of CaMKII in single dendritic spines during long-term potentiation. Nature *458*, 299–304. https://doi.org/10.1038/nature07842.

39. Otmakhova, N.A., Otmakhov, N., Mortenson, L.H., and Lisman, J.E. (2000). Inhibition of the cAMP pathway decreases early long-term potentiation at CA1 hippocampal synapses. J. Neurosci. *20*, 4446–4451. https://doi.org/10.1523/JNEUROSCI.20-12-04446.2000.

40. Sutton, M.A., and Schuman, E.M. (2006). Dendritic protein synthesis, synaptic plasticity, and memory. Cell *127*, 49–58. https://doi.org/10.1016/j.cell.2006.09.014.

41. Otmakhov, N., Griffith, L.C., and Lisman, J.E. (1997). Postsynaptic inhibitors of calcium/calmodulin-dependent protein kinase type II block induction but not maintenance of pairing-induced long-term potentiation. J. Neurosci. *17*, 5357–5365. https://doi.org/10.1523/JNEUROSCI.17-14-05357.1997.

42. Lisman, J., and Spruston, N. (2005). Postsynaptic depolarization requirements for LTP and LTD: a critique of spike timing-dependent plasticity. Nat. Neurosci. *8*, 839–841. https://doi.org/10.1038/nn0705-839.

43. Asrican, B., Lisman, J., and Otmakhov, N. (2007). Synaptic strength of individual spines correlates with bound Ca^{2+}–calmodulin-dependent kinase II. J. Neurosci. *27*, 14007–14011. https://doi.org/10.1523/JNEUROSCI.3587-07.2007.

44. Miningou Zobon, N.T., Jędrzejewska-Szmek, J., and Blackwell, K.T. (2021). Temporal pattern and synergy influence the activity of ERK signaling pathways during L-LTP induction. Elife *10*, e64644. https://doi.org/10.7554/eLife.64644.

45. Dorman, D.B., and Blackwell, K.T. (2022). Synaptic plasticity is predicted by spatiotemporal firing rate patterns and robust to in vivo-like variability. Biomolecules *12*, 1402. https://doi.org/10.3390/biom12101402.

46. Fujii, H., Inoue, M., Okuno, H., Sano, Y., Takemoto-Kimura, S., Kitamura, K., Kano, M., and Bito, H. (2013). Nonlinear decoding and asymmetric representation of neuronal input information by CaMKIIα and calcineurin. Cell Rep. *3*, 978–987. https://doi.org/10.1016/j.celrep.2013.03.033.

47. Singh, D., and Bhalla, U.S. (2018). Subunit exchange enhances information retention by CaMKII in dendritic spines. Elife *7*, e41412. https://doi.org/10.7554/eLife.41412.001.

48. Chang, J.Y., Parra-Bueno, P., Laviv, T., Szatmari, E.M., Lee, S.J.R., and Yasuda, R. (2017). CaMKII autophosphorylation is necessary for optimal integration of Ca^{2+} signals during LTP induction, but not maintenance. Neuron *94*, 800–808.e4. https://doi.org/10.1016/j.neuron.2017.04.041.

49. Murakoshi, H., Wang, H., and Yasuda, R. (2011). Local, persistent activation of Rho GTPases during plasticity of single dendritic spines. Nature *472*, 100–104. https://doi.org/10.1038/nature09823.

50. Inouye, S., Ogawa, H., Yasuda, K., Umesono, K., and Tsuji, F.I. (1997). A bacterial cloning vector using a mutated Aequorea green fluorescent protein as an indicator. Gene *189*, 159–162. https://doi.org/10.1016/S0378-1119(96)00753-6.

51. Argunşah, A.Ö., Erdil, E., Ghani, M.U., Ramiro-Cortés, Y., Hobbiss, A.F., Karayannis, T., Çetin, M., Israely, I., and Ünay, D. (2022). An interactive time series image analysis software for dendritic spines. Sci. Rep. *12*, 1–15. https://doi.org/10.1038/s41598-022-16137-y.

52. Stoppini, L., Buchs, P.A., and Muller, D. (1991). A simple method for organotypic cultures of nervous tissue. J. Neurosci. Methods *37*, 173–182. https://doi.org/10.1016/0165-0270(91)90128-M.

53. Heeger, D. (2000). Poisson Model of Spike Generation, Lecture Notes (New York University). https://www.cns.nyu.edu/~david/handouts/poisson.pdf.

STAR★METHODS

KEY RESOURCES TABLE

REAGENT or RESOURCE	SOURCE	IDENTIFIER
Bacterial and virus strains		
Afp-GFP plasmid	Inouye et al.[50]	N/A
Chemicals, peptides, and recombinant proteins		
MNI-caged-L-glutamate	TOCRIS	CAS No: 295325-62-1; Batch No: 40A/160038, 36A/147239, 35A/140571, 32A/127489, 32A/133545, 43A/174380, 40A/165397
Cycloheximide	TOCRIS	CAS No: 66-81-9
Anisomycin	TOCRIS	CAS No: 22862-76-6; Batch No: 9A/172390, 7A/144486
APV	TOCRIS	CAS No: 79055-68-8
Tetrodotoxin citrate (TTX)	TOCRIS	CAS No: 18660-81-6 Batch No: 43C, 43b, 45A
Biocytin Alexa Fluor™ 594	ThermoFisher	CAS No: A-12922
Experimental models: Organisms/strains		
Mouse: C57BL/6J	The Jackson Laboratory	RRID:IMSR_JAX:000664
Software and algorithms		
Ultima *In Vitro* Multiphoton Microscope System	Bruker	https://www.bruker.com/products/fluorescence-microscopes/ultima-multiphoton-microscopy/ultima-in-vitro/overview.html; RRID:SCR_017142
Matlab	MathWorks	http://www.mathworks.com/products/matlab/; RRID:SCR_001622
pClamp 10	Molecular Devices	http://www.moleculardevices.com/products/software/pclamp.html/; RRID:SCR_011323
Dendritic spine segmentation and analysis	Argunsah et al.[51]	https://doi.org/10.5281/zenodo.7871556
Naturalistic pattern generator for glutamate uncaging	This study	https://doi.org/10.5281/zenodo.7871541

RESOURCE AVAILABILITY

Lead contact

Further information and requests for resources and reagents should be directed to and will be fulfilled by the lead contact, Inbal Israely (inbal@uw.edu).

Materials availability

This study did not generate new unique reagents.

Data and code availability

- All data reported in this paper will be shared by the lead contact upon request.
- All original code has been deposited at Zenodo and is publicly available as of the date of publication. DOIs are listed in the key resources table.
- Any additional information required to reanalyze the data reported in this paper is available from the lead contact upon request.

EXPERIMENTAL MODEL AND SUBJECT DETAILS

Experimental animals

All animal experiments were carried out in accordance with European Union regulations on animal care and use, and with the approval of the Portuguese Veterinary Authority (DGV). Cultured hippocampal slices were prepared from postnatal day 7–10C57BL/6J mice.[52] Both male and female mice are used.

METHOD DETAILS

Preparation of organotypic slice cultures

350 μm thick slices were made with a chopper in ice-cold ACSF containing 2.5 mM KCl, 26 mM $NaHCO_3$, 1.15 mM NaH_2PO_4, 11 mM D-glucose, 238 mM sucrose, 1 mM $CaCl_2$, and 5 mM $MgCl_2$, and cultured on membranes (Millipore). The slices were maintained in an interface configuration with the following media: 1×MEM (Invitrogen), 20% horse serum (Invitrogen), GlutaMAX 1 mM (Invitrogen), 27 mM D-glucose, 30 mM HEPES, 6 mM $NaHCO_3$, 1 mM $CaCl_2$, 1 mM $MgSO_4$, 1.2% ascorbic acid, 1 μg/ml insulin. The media was changed every 2 to 3 days. The pH was adjusted to 7.3, and osmolarity was adjusted to 300–310 mOsm. All chemicals were from Sigma unless otherwise indicated.

Biolistic gene transfection

Slice cultures were transfected using a Helios gene gun (Bio-Rad) after 4–5 days *in vitro* (DIV). Gold beads (10 mg, 1.6 μm diameter, Bio-Rad) were coated with 100 μg Afp-GFP plasmid DNA[50] according to the manufacturer's protocol and delivered biolistically into the slices at 160-200 psi. Experiments were performed 3–7 days post-transfection, beginning at DIV 7.

Patch clamp Electrophysiology

Hippocampal slice cultures were pre-incubated for 45min to 1h at room temperature and perfused continuously with ACSF. Whole-cell voltage-clamp recordings were performed in CA1 pyramidal neurons, using 7–8 MΩ electrodes filled with an internal solution containing: 136.5 mM K-gluconate, 9 mM NaCl, 17.5 mM KCl, 10 mM HEPES, 0.2 mM EGTA, pH adjusted to 7.2 with KOH, and 284 mOsm. Cells were voltage-clamped at −65 mV. Cellular recordings in which series resistance was higher than 25 MΩ were discarded, and stability was assessed throughout the experiment (±20%). Alexa 594 at 0.025 mM was added to the internal solution to visualize dendritic spines. uEPSC responses were evoked by glutamate uncaging (see below). Signals were acquired using a Multiclamp 700B amplifier (Molecular Devices), and data were digitized with a Digidata 1440 at 3 kHz. EPSC amplitudes were analyzed using custom software written in Matlab.

Generation of naturalistic stimulation patterns

We utilized a technique for generating spike sequences with inter-spike-interval distribution satisfying a Poisson process. The distribution of inter-event-intervals in a homogeneous Poisson process follows an exponential distribution, as shown in Heeger et al.[53]Equation 7. To generate a random variable that conforms to a given distribution, one can apply a uniform distribution to the inverse function of the cumulative distribution (inverse transform sampling). In our case, we generated 10000 patterns by applying this technique with a rate of $r = 0.5$ (Hz) spanning 60s. Specifically, we generated interspike interval patterns from a uniform distribution between 0 and 1, and applied the inverse transform sampling using the inverse function of the exponential distribution shown in Heeger et al.[53]Equation 7, which is $-\log(x) / r$. Here, x is a random number between 0 and 1, drawn from a uniform distribution (n=30 stimuli drawn). We then generated pulse times t(i) iteratively from the formula $t(i+1) = t(i) - \log(x)/r$, where t(i) represents the time of the current stimulus (i), and $t(i+1)$ represents the time at the next stimulus $(i+1)$. It's important to note that $-\log(x)/r$ is a positive number for $0<x<1$. The use of a uniform distribution for x ensures that the inter-event intervals are random and unpredictable. A link to the code used to generate the naturalistic patterns for plasticity experiments is available in the key resources table. This code is inspired by the code accompanied by the lecture notes of David Heeger's Poisson Model of Spike Generation.[53]

Two-photon imaging and uncaging

Two-photon imaging was performed at 910 nm using a galvanometer-based scanning system (Prairie Technologies, acquired by Bruker Corporation) on a BX61WI Olympus microscope, using a Ti:Sapphire laser (Coherent Inc.) controlled by PrairieView software. Slices were perfused with oxygenated ACSF containing 127 mM NaCl, 2.5 mM KCl, 25 mM $NaHCO_3$, 1.25 mM NaH_2PO_4, 25 mM D-glucose, 2 mM $CaCl_2$ and 1 mM $MgCl_2$ (equilibrated with O_2 95%/CO_2 5%) at 38°C to achieve room temperature in the chamber at a rate of 1.5 ml/min. Imaging was started 45 min to 1 h after slice incubation began. Secondary or tertiary dendrites of CA1 neurons were imaged using a water immersion objective (60X, 0.9 NA, Olympus) with a digital zoom of 10X. Z-stacks (0.3 μm per section) were collected once every 5 min for up to 4 hours at a resolution of 1024×1024 pixels, resulting in a field of view approximately 20μm×20μm. Imaging laser power and PMT gain settings were kept constant throughout each experiment. Caged glutamate was calibrated as

previously described and briefly as follows.[8,26] MNI-caged-L-glutamate (MNI-Glu) (Tocris) was reconstituted in the dark in aCSF lacking $MgCl_2$ or $CaCl_2$ to make a 10 mM stock solution. Individual aliquots were diluted to the working concentration of 2.5 mM MNI-Glu in 3 ml final volumes to obtain the uncaging aCSF solution and supplemented with $MgCl_2$ or $CaCl_2$ at the start of each experiment. We verified the concentration of each batch of reconstituted MNI-Glu by delivering five 1ms-long test pulses to single spines and recording uEPSCs by whole cell patch clamp recordings. Average spontaneous mEPSC amplitudes were used to determine the power required to produce an uEPSC of comparable size (at the back aperture). One aliquot of uncaging ACSF was delivered in a closed recirculation setting per plasticity experiment to maintain stable MNI-Glu concentrations. To induce plasticity, each uncaging pattern tested was applied to a single spine by positioning the laser 0.5 μm from the tip of the spine head in the presence of uncaging MNI-glutamate (2.5 mM) and delivering 4ms-long laser pulses at a power of 30mW (at 720nm). Glutamate uncaging was done in the absence of extracellular Mg^{2+} to allow for the observation of long-lasting structural changes without washing out plasticity-related proteins during whole-cell physiology.[28] Stimulations were carried out at spines located on secondary or tertiary dendrites within the stratum radiatum of CA1 pyramidal neurons sparsely labeled with GFP using gene gun. The region containing the stimulated spine and unstimulated neighbors was imaged every 5 minutes for a baseline period of 20 minutes, a selected spine underwent uncaging stimulation for 60s, and the dendritic region was subsequently imaged every 5 minutes for up to 4 hours in ACSF containing 0.5μM TTX (Figure 2A). In some experiments, uncaging was carried out while cells underwent whole-cell patch clamp recordings to determine whether each pulse would reach the soma (Figures 1D and S2). In this experiment, uncaging ACSF was recirculated, and several spines were selected for stimulation. We carried out the sequential stimulation of spines, first by stimulating NSP-Uni at each one, followed by NSP-Beg at those same spines, and finally by delivering NSP-End to the same spines.

QUANTIFICATION AND STATISTICAL ANALYSIS

All analyses were performed using Matlab (MathWorks). We quantified changes in spine volume using a Matlab-based toolbox that we developed, called SpineS,[51] in which the semi-automatic segmentation of spine heads occurs in an unbiased manner (Figures 2B and S3). All normalization was performed on a per-spine basis as a percent of the average baseline value for that spine. We imaged a dendrite of interest every 5 minutes and analyzed it in 15min bins. Results are presented as mean ± SEM. All statistical analyses were performed using custom code written in Matlab (MathWorks). The Nonparametric Mann-Whitney U test was used to compare spine volumes at any time bin versus baseline or different conditions. Time series were compared using repeated-measures ANOVA. Stars (*) represent degrees of significance as follows: (*) = $p < 0.05$; (**) = $p < 0.01$; (***) = $p < 0.001$).